Research Article | Vol. 27, No. 5 | 4 Mar 2019 | OPTICS EXPRESS 6377
Optics EXPRESS

Technique for the measurement of picosecond optical pulses using a non-linear fiber loop mirror and an optical power meter

UMAIR A. KORAI,[1,2,*] ZIFEI WANG,[3] COSIMO LACAVA,[4] LAWRENCE R. CHEN,[3] IVAN GLESK,[1] AND MICHAEL J. STRAIN[5]

[1]*Department of Electronic and Electrical Engineering, University of Strathclyde, Glasgow G1 1XW, UK*
[2]*Department of Telecommunication Engineering, Mehran University of Engineering and Technology, Jamshoro 72060, Pakistan*
[3]*Department of Electrical and Computer Engineering, McGill University, Montreal H3A 0E9, Canada*
[4]*Optoelectronics Research Centre, University of Southampton, Southampton SO17 1BJ, UK*
[5]*Institute of Photonics, Dept. of Physics, University of Strathclyde, Glasgow G1 1RD, UK*
[*]*umair.korai@faculty.muet.edu.pk*

Abstract: A method for measuring picosecond pulse width by using only fiber components and optical power meters is presented. We have shown that the output power splitting ratio of a non-linear fiber loop mirror can be used to extract the full-width half maximum of the optical pulse, assuming a known slowly varying envelope shape and internal phase structure. Theoretical evaluation was carried out using both self-phase and cross-phase modulation approaches, with the latter showing a twofold sensitivity increase, as expected. In the experimental validation, pulses from an actively fiber mode-locked laser at the repetition rate of 10 GHz were incrementally temporally dispersed by using SMF–28 fiber, and then successfully measured over a pulse width range of 2–10 ps, with a resolution of 0.25 ps. This range can be easily extended from 0.25 to 40 ps by selecting different physical setup parameters.

1. Introduction

The efficient generation of ultra-short laser pulses in the picosecond regime has enabled a wide range of applications from optical communications [1] to the measurement of ultra-fast physical processes [2]. In order to measure the characteristics of picosecond optical fields, a number of techniques have been developed including frequency resolved optical gating (FROG) [3–5], spectral phase interferometry for direct electric-field reconstruction of ultra-short optical pulses (SPIDER) [6,7] and sonogram [8,9]. Some modified versions of FROG have also been reported using cross phase modulation and four wave mixing for the full characterization of an optical pulse [10,11]. In addition to these non-linear methods, there are a number of linear self referencing methods, for example, phase reconstruction using optical ultrafast differentiation (PROUD), that avoid the requirement of high pump powers and provide a complete pulse characterization [12–14]. These methods allow for the full amplitude and phase reconstruction of the pulse. Compact methodologies based on on-chip technologies have also been demonstrated making use of highly non-linear optical waveguide technology [15,16]. In general, ultra-short pulse measurement techniques either require high pulse energies or expensive measurement equipment such as optical spectrometers in order to operate.

All optical performance monitoring is crucial for achieving stable optical networks, in particular with regards to the effects of dispersion. There are several parameters that can alter the dispersion of an optical link, i.e. temperature, path reconfiguration or physical maintenance around the fiber site [17]. Also, in some applications, for example in optical networks or in cases where well-behaved optical pulses are used as a temporal probe, it is

#354719 https://doi.org/10.1364/OE.27.006377
Journal © 2019 Received 7 Dec 2018; revised 2 Feb 2019; accepted 3 Feb 2019; published 20 Feb 2019

Optics EXPRESS

often enough to monitor the temporal envelope of the pulse to allow compensation of any dispersion that may be induced between the laser source and the monitor point. High-speed photodetectors and sampling oscilloscopes, intensity auto-correlators or cross-correlators can be used in laboratory environments for this purpose.

In this manuscript, we present an alternative method which uses a fiber amplifier, non-linear optical fiber loop mirror (NOLM) [18] and optical power meters. Since the system is implemented in an all-fiber configuration, with no moving parts or complex measurement equipment, it can be implemented as a simple system bolt-on, or in remote locations with the potential for distributed arrays of monitors across networks. Unlike optical sampling oscilloscopes and optical auto-correlators, this method does not monitor the shape of the optical pulses but only their temporal width; hence, it can also be used to monitor the residual dispersion of the optical link [17].

Design of the method was carried out using simulations of the non-linear Schrodinger equation(s) using well-defined split step method [19]. From simulations we found that this method is compatible with well-behaved pulses with slowly varying envelopes such as sech^2 or Gaussian. The measurement range is related to the non-linear phase shift introduced by the measured signal (its peak power can be boosted by using an erbium-doped fiber amplifier (EDFA) up to its saturated output power) and to the length of the non-linear medium and its non-linear coefficient. In this work, pulse widths up to 10 ps are measured, with a resolution of 0.25 ps, assuming a sech^2 or Gaussian pulse envelope with slowly varying phase internal structure. The measurement range can be extended to cover 0.25 to 40 ps by careful selection of the physical parameters in the setup.

The remainder of this paper is organized as follows: Section 2 describes the highly non-linear fiber (HNLF) based NOLM pulse width measurement scheme and the simulated model using the split-step method for both, self-phase and cross-phase modulation variations. Section 3 presents the experimental realization of the scheme with results and analysis presented in section 4. Device limitations and discussion are presented in section 5 and finally conclusions are presented in section 6.

2. Picosecond pulse width measurement using non-linear optical loop mirror

As noted in the introduction, the method presented here relies on the assumption that the optical picosecond pulses under investigation are of a simple form with typically a sech^2 or Gaussian shape and little internal phase structuring. The purpose of this method is to provide a means to monitor pulse width variation induced, for example by dispersion between the pulse origin and monitor point. We present two variations of the measurement technique, both based on a χ^3 optical non-linearity process in a NOLM (see Fig. 1). In both approaches optical pulses are coupled to the NOLM and the resulting average power at its output ports is measured using a slow optical power meters. The ratio $\frac{P_{out1}}{P_{out2}}$ of the measured average output powers is a function of the optical switching induced by either self-phase or cross-phase modulation depends on the peak power of a laser pulse injected into the NOLM. For well-behaved pulses, the peak power is simply related to average power through the envelope shape and pulse train duty cycle. In order to over-sample the measurement, the input pulses are incrementally amplified by an erbium doped fiber amplifier (EDFA) to produce a series of power splitting ratios as a function of the measured average power of the input pulse train.

The system behavior can be modelled by the non-linear Schrodinger equation, numerically solved using a split-step method [19]. Input values to this numerical method were chosen to match parameter values of HNLF and are summarized in Table 1. The repetition rate of the pulse source was taken as 10 GHz, matching the erbium doped fiber mode-locked laser source used in the experiments. In this manuscript we use a non-linear fiber length of 100 m and an EDFA with a saturated power level of 17 dBm and therefore simulations are

Optics EXPRESS

carried out to demonstrate the performance of the system under these constraints. However, the achievable pulse width measurement range of the method can be tuned by varying the setup components, discussed in more detail in section 5.

Table 1. HNLF simulation parameters.

Parameter	Value	Unit
Length (L_{HNLF})	100	m
Gamma (γ)	10.8	$(W\ km)^{-1}$
Dispersion (D)	0.11	ps/nm/km
Dispersion slope (S)	0.016	$ps/nm^2/km$
Absorption coefficient (α)	0.9	dB/km
Splice Loss (HNLF to SMF28)	0.2	dB

2.1. Self-phase modulation

Figure 1(a) shows the self-phase modulation (SPM) variant of the scheme. In this case, the amplified pulse train (P_{signal}) is coupled in to one port of the NOLM, where the coupler ratio is unbalanced (80:20) in order to create asymmetry in the counter-propagating modes. An additional optical attenuator (10 dB) is added to the loop to give control of this imbalance. The higher power replica of the pulse undergoes SPM in the HNLF creating a phase shift between the replicas as they recombine at the output coupler.

The proportion of the total power coupled to each port is dependent on the relative phase between the two pulse replicas, and their relative powers:

$$P_{out} = \begin{pmatrix} P_{out1} \\ P_{out2} \end{pmatrix} = \begin{pmatrix} n_1 \\ n_2 \end{pmatrix} P_{in} \tag{1}$$

where,

$$n_1 = e^{\phi_L}\sqrt{p(1-p)}(1+e^{j\theta_{NL}})e^{j\frac{\pi}{2}} \tag{2}$$

$$n_2 = e^{\phi_L}(pe^{j\theta_{NL}} - (1-p)) \tag{3}$$

ϕ_L includes the linear phase shift and linear loss and can be computed as $\phi_L = j\beta L_{HNLF} - \alpha L_{HNLF}$, β is the propagation constant of the field in the optical fiber, α is the linear absorption loss, p is the splitting ratio of the input coupler, and L_{HNLF} is the length of the HNLF. θ_{NL} is the non-linear phase shift and is proportional to the input power. The Eqs. (2) and (3) are modified from [21] due to the inclusion of a coarse wavelength division multiplexer (CWDM) coupler to inject the amplified pulse train into the loop mirror. The non-linear phase shift can be computed by numerically solving the non-linear Schrodinger equation(s), (4) for SPM and (5) and (6) for XPM, using the split step method where the non-linear phase shift induced by cross phase modulation (XPM) is approximately twice that accumulated through SPM [19].

$$\frac{\partial A}{\partial z} + \frac{i\beta_2}{2}\frac{\partial^2 A}{\partial T^2} = i\gamma|A|^2 A - \frac{\alpha}{2}A \tag{4}$$

$$\frac{\partial A_a}{\partial z} + \frac{i\beta_{2a}}{2}\frac{\partial^2 A_a}{\partial T^2} = i(\gamma|A_a|^2 + 2\gamma|A_b|^2)A_a - \frac{\alpha}{2}A_a \tag{5}$$

$$\frac{\partial A_b}{\partial z} + \frac{i\beta_{2b}}{2}\frac{\partial^2 A_b}{\partial T^2} = i(\gamma|A_b|^2 + 2\gamma|A_a|^2)A_b - \frac{\alpha}{2}A_b \tag{6}$$

Optics EXPRESS

Where, the subscript '*a*' shows the high power signal parameters and '*b*' shows the low power continuous wave probe signal. $A_{(a,b)}$ is the slowly varying amplitude of the pulse envelope, $\beta_{2(a,b)}$ is the group velocity dispersion, $\gamma_{(a,b)}$ is the non-linear coefficient, $\lambda_{(a,b)}$ is the operating wavelength and α is the linear loss of the waveguide. The values of all the above parameters are summarized in Table 1. The splice loss and the absorption has already included in the experimental results; hence both are not included in the simulations.

The effect of counter propagating non-linear interactions in the NOLM can be significant when using high repetition rate signals [20], hence the total effective non-linear phase shift using SPM and XPM, by taking the counter clockwise non-linear phase shift into account, can be calculated using Eq. (7).

$$\Delta\theta_{eff} = \theta_{cw\_NL} - \theta_{ccw\_NL} \tag{7}$$

Where $\Delta\theta_{eff}$ is the total effective phase shift, θ_{cw_NL} is the non-linear phase shift produced in the clockwise direction and θ_{ccw_NL} is the non-linear phase shift produced in counter-clockwise direction due to XPM.

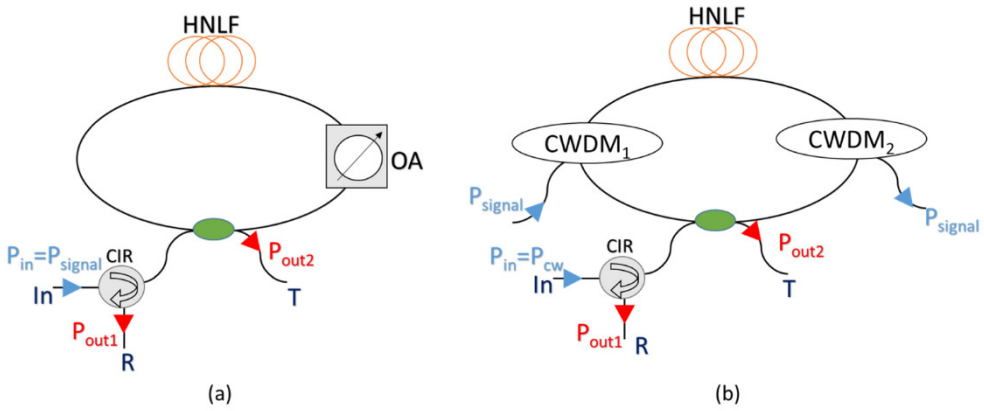

Fig. 1. Non-linear optical loop mirror (a) in self phase modulation configuration; (b) in cross phase modulation configuration using CWDM couplers for injecting and filtering out the pulsed signal. Where OA – optical attenuator, CWDM – course wavelength division multiplexing/de-multiplexer, CIR – optical circulator, and HNLF – highly non-linear fiber

Figures 2(a) and 2(b) shows the normalized reflected power (P_{out1}) at the reflected port (*R*) and transmitted power (P_{out2}) at transmitted port (*T*) of NOLM plotted as a function of the input average power (P_{in}), with the pulse width as a parameter. An optical circulator (CIR) is used for separating the input and output reflected power of the NOLM. A sech^2 pulse envelope is assumed in this case. The output powers follow sinusoidal variations as a function of the input average power for a given input pulse width, with maximum and minimum values defined by the asymmetric coupling fraction of the input/output coupler. The input average power inducing a $\pi/2$ phase-shift results switching of power between *R* and *T* ports of the NOLM and subsequently can be used to extract the pulse width from measurements of the power splitting between *R* and *T* ports as a function of P_{in}, as shown in Fig. 2(c). The relationship between pulse widths and $\pi/2$ switching point can be adequately fitted to a second order polynomial. It is also apparent that to achieve this switching, average powers in the range of 10's of mW are required for few picosecond pulses. This limits the useful range of this method to pulses of ~5 ps with our EDFA having a saturated power of ~50 mW (17 dBm).

Optics EXPRESS

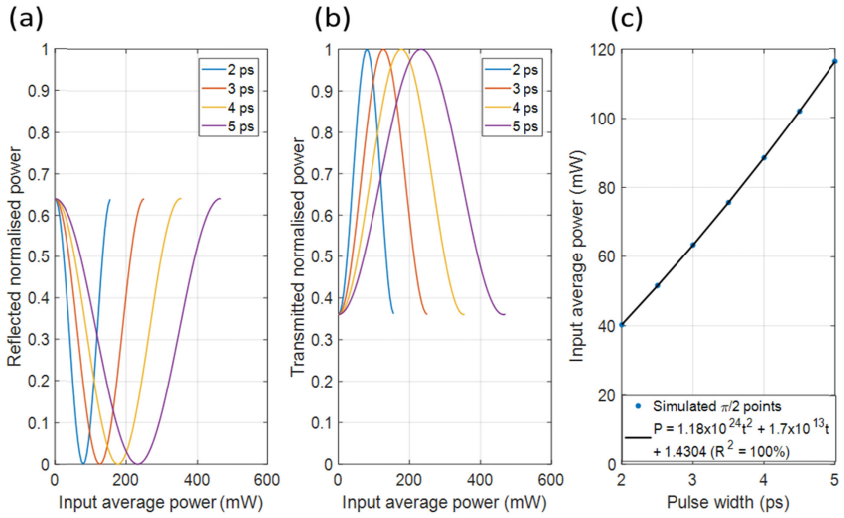

Fig. 2. Simulated NOLM output power at (a) reflected, (**b**) transmitted port as a function of input average power of the signal for different pulse widths using SPM. (c) The input average power at π/2 switching points as a function of pulse width.

2.2. Cross-phase modulation

With a minor modification of the setup in Fig. 1(a), the sensitivity of the SPM scheme can be significantly enhanced. Figure 1(b) shows a setup that includes a secondary CW laser source as a probe of the loop non-linearity in a XPM scheme. In this case, the probe signal is coupled in to one input port of NOLM and the pulse train is added to travel the NOLM only in one direction using a CWDM. The probe signal experiences strong XPM in one of the counter propagating modes, inducing a relative phase shift between the modes at the output coupler. In order to avoid cross-talk at the detectors, the pulse train is coupled out of the loop, using a second CWDM, before reaching the output coupler.

The average output power at the port *T* and *R,* respectively can be calculated using (1), (2), and (3), where in this case the non-linear phase shift is directly proportional to the loop entering peak power (P_{signal}), with the signal pulse width as a parameter. As before, the reduced relative phase shift between clockwise and counter-clockwise signals is taken into account using Eq. (7). Figures 3(a) and 3(b) show the normalized transmitted and reflected output powers of the probe as a function of input average power of the pulse train for different pulse widths. As expected, the $\pi/2$ switching points are reached at half the power in the XPM case as compared to the SPM. Figure 3(c) shows the quadratic fit of the $\pi/2$ points for the XPM setup.

Optics EXPRESS

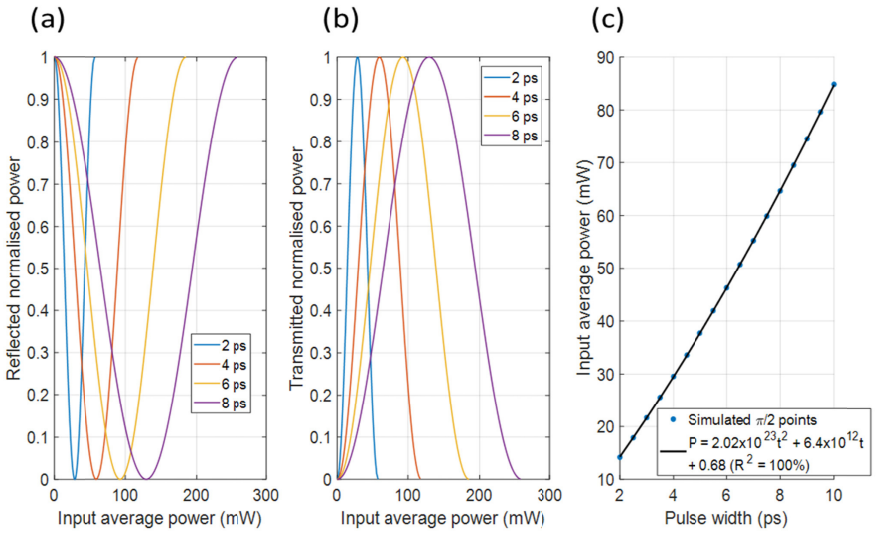

Fig. 3. Simulated NOLM output power at: (a) reflected, (b) transmitted port as a function of input average power of the signal for different pulse widths using XPM. (c) The input average power at $\pi/2$ points as a function of pulse width of the signal and their fitting.

2.3. Effect of pulse envelope function

The XPM simulations were then performed for a Gaussian pulse envelope, where the $\pi/2$ switching points as a function of the laser pulse width and are compared with the previously obtained sech^2 case in Fig. 4. There is not a noticeable difference between those two results, meaning that calibration of the experimental setup with either pulse shape would allow measurement of both envelope types with the same accuracy.

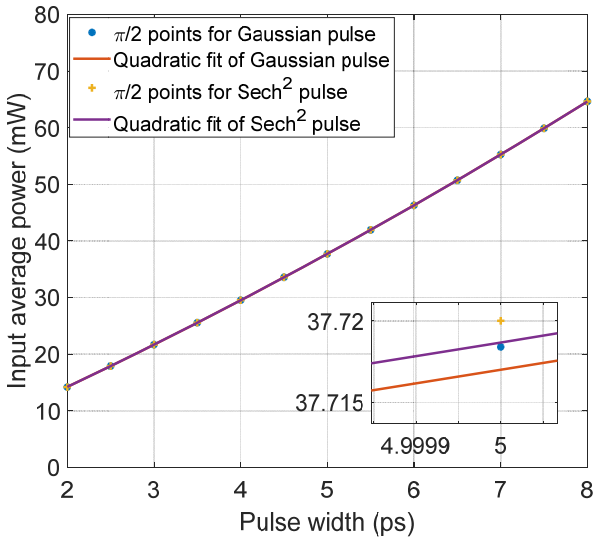

Fig. 4. Quadratic fitted $\pi/2$ points for both Gaussian and sech^2 pulse shapes as a function of input pulse width.

3. Experimental setup for measurement of pulse width

Schematics of the experimental setups used for measurement of optical pulse widths using NOLM based on SPM and XPM are shown in Figs. 5(a) and 5(b), respectively. The PriTel, Inc. mode-locked fiber laser running at a 10 GHz repetition rate was used as a source of

Optics EXPRESS

picosecond optical pulses, referred here as the signal. The central wavelength of the signal was 1550.7 nm with a spectral bandwidth of 1.4 nm. The signal was amplified using an EDFA limited to a saturated output power of 50 mW (17 dBm). The input pulse width variation was achieved by using serially coupled lengths of SMF28 patchcord cables to disperse the signal. For the XPM setup, a low power continuous wave (CW), referred to here as the probe, was generated using Agilent 81989A tunable laser at the wavelength of 1530 nm with a power of 5 mW. A 1% power tap was introduced before the NOLM for an input average power monitoring of the signal by a temperature stable Agilent 8153A Lightwave Multimeter. The probe was then injected into the NOLM via a 50:50 optical directional coupler and the signal via $CWDM_1$ coupler (see Fig. 5(b)). The two polarization controllers (PC) used in the setup were set to maximize the power coupled to the reflected port in the linear regime. Once the state of PCs was set, it was not altered for any of the subsequent measurements. The passband of the $CWDM_1$ coupler is 1541 to 1559 nm. The signal after traveling HNLF of length (L_{HNLF}) was subsequently filtered out of the loop using $CWDM_2$ coupler with the passband of 1542 to 1558 nm. The transmitted and reflected average power of the probe were measured at *T* and *R* ports, respectively as indicated in Fig. 5(b). The pulse width of the signal was measured using a FR-103XL optical auto-correlator before entering in to the NOLM.

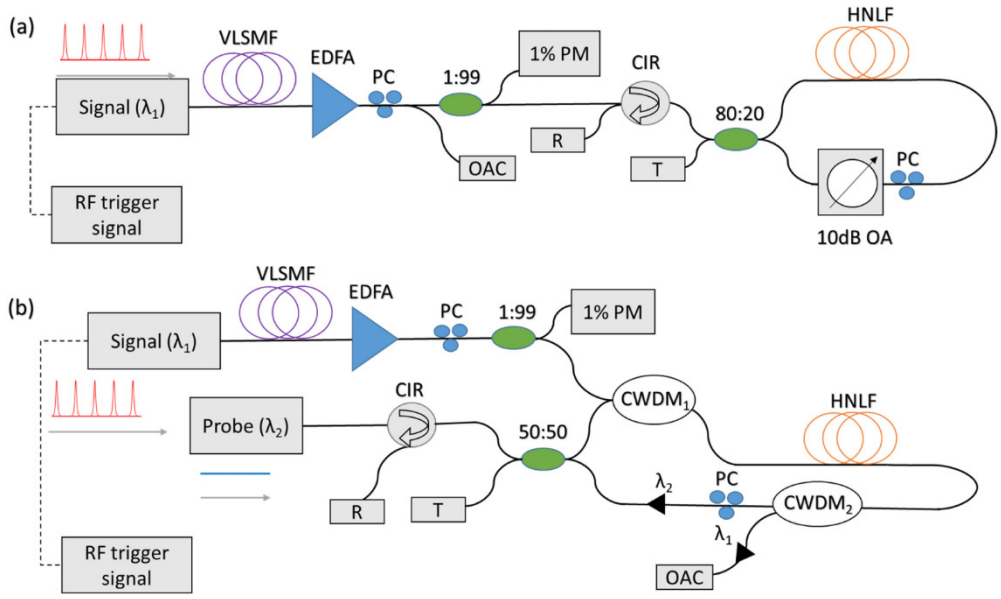

Fig. 5. Experimental setup for optical pulse width measurement using NOLM based on: (a) SPM and (b) XPM, respectively. Where, PM – power meter, CIR – optical circulator, OAC – optical auto-correlator, EDFA – erbium doped fiber amplifier, PC – polarization controller, CWDM – course wavelength division multiplexer/de-multiplexer, HNLF – highly non-linear fiber, OA – optical attenuator, VLSMF – variable length single mode fiber, R – reflected port, T – transmitted port.

4. Experimental results

4.1. NOLM based on self-phase modulation configuration

The experimental setup for optical pulse width measurements using the NOLM based on SPM is shown in Fig. 5(a). A varying length of SMF28 optical fiber was used to disperse nearly transform limited 2 ps FWHM laser pulses to 2.9 ps, 3.7 ps, and 4.5 ps, respectively. Figure 6 shows the normalized optical power obtained from measurements at *R* and *T* ports as

Optics EXPRESS

a function of the P_{in}, for the case of a 2 ps pulse. Since the simulated curves show sinusoidal dependence on the input average power, hence the measured transmitted and reflected data was fitted to (8) and (9), respectively, where *A*, *B*, *C,* and *D* are free parameters. This fitting then allows extraction of the $\pi/2$ point.

$$P_{OTX} = A.\sin(B.P_{in} + C) - D \tag{8}$$

$$P_{ORX} = 1 - P_{OTX} \tag{9}$$

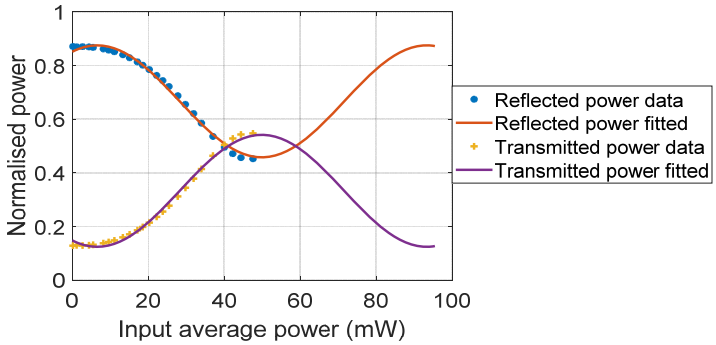

Fig. 6. The normalized reflected and transmitted NOLM output power based on SPM measurements showing a sinusoidal fit using (8) and (9) to extract the $\pi/2$ point

The experimentally measured and fitted transmission and reflection powers of the NOLM obtained for up to a 50 mW of the input average optical power are shown in Figs. 7(a) and 7(b), respectively. A 10 dB optical attenuator is used in the counter clockwise direction in order to suppress the power of signal hence the signal power in the 20% arm is not enough to produce the non-linearity. For wider pulses, the $\pi/2$ points were not accessible experimentally due to limited available EDFA saturated power, hence the fitting curves based on (8) and (9) were used to obtain the $\pi/2$ points. Figure 7(c) shows the input average power at $\pi/2$ points and the quadratic fitting. The measured curves show good agreement with the simulations and a clear dependence on the input pulse width.

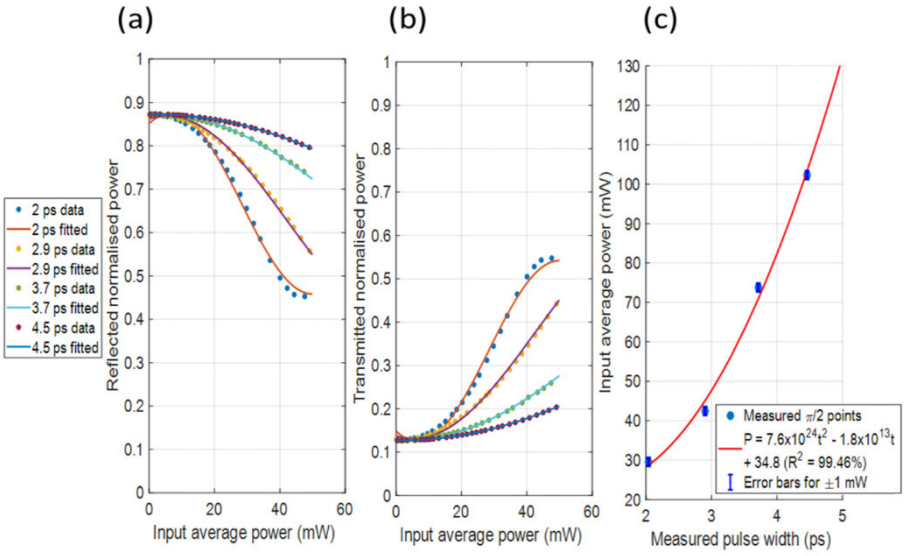

Fig. 7. Measured: (a) reflected, (b) transmitted output power of the NOLM in SPM configuration as a function of the input average power of the signal obtained for different pulse

Optics EXPRESS

width values. (c) Input average power at $\pi/2$ points as a function of the signal pulse showing the quadratic fitting.

4.2. NOLM based on cross phase modulation configuration

The experimental setup for optical pulse width measurements using the NOLM based on XPM configuration is shown in Fig. 5(b). Similarly, as before, five different pulse widths were generated from the initial 2 ps FWHM pulses. Again, the measured data were fitted to a sinusoidal function described by using (8) and (9). The 2ps pulse data were only fitted up to the $\pi/2$ point, as after this the switching exhibited some saturation.

The normalized transmission and reflection output powers of the XPM based NOLM are shown in Figs. 8(a) and 8(b), respectively. The input average power of the signal at $\pi/2$ points and the quadratic fitting is shown in Fig. 8(c).

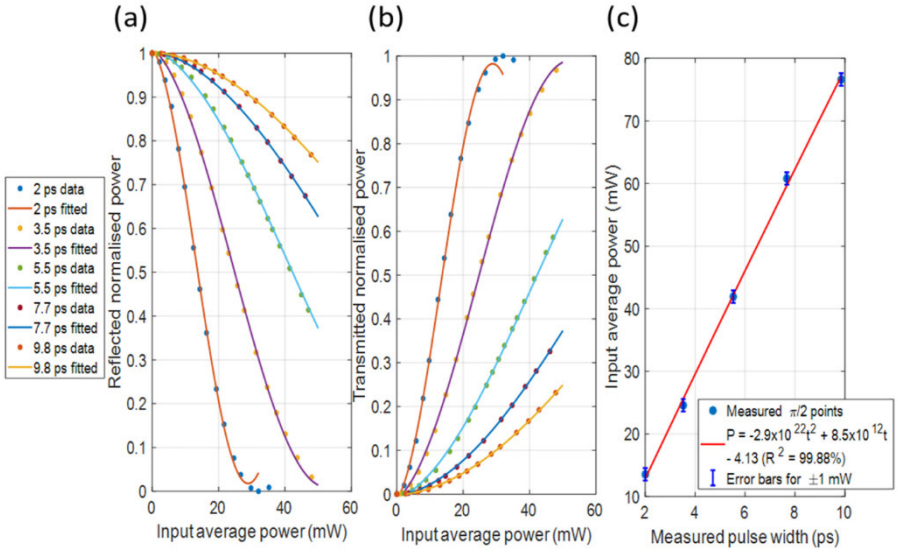

Fig. 8. Measured: (a) reflected, (b) transmitted output power of the NOLM on XPM configuration as a function of the input average power of the signal obtained for different pulse widths values. (c) Input average power at $\pi/2$ points as a function of the signal pulse showing quadratic fitting.

As predicted by the theory, the sensitivity of the XPM is doubled compared with the SPM case, thus allowing more efficient pulse width measurements. We measured the input average optical power of the signal with an accuracy of ± 1 mW, that together with the R^2 = 99.88% of the quadratic fit, gives a predicted pulse width resolution of ~0.25 ps.

5. Device limitations and discussion

In order to characterize the temporal width of an optical pulse, the setup described above is required to define the $\pi/2$ switching point with respect to the average power of the signal. This therefore puts a limitation on the measurement range of the system that depends on the available saturation power of the EDFA and the length of non-linear fiber in the loop. As stated above, the accuracy of the measurement is limited by the accuracy of measuring the input average power from power meter and the linearity of the fitted calibration curve. Assuming the dispersion length is higher than the non-linear length, the non-linear phase shift for XPM is given as:

$$\phi_{XPM} = \frac{2\gamma P_{av} T L_{eff}}{\tau} \tag{10}$$

Optics EXPRESS

where γ is the non-linear coefficient, P_{av} is the input average power, T is the laser repetition period, τ is the pulse width of the laser signal, and L_{eff} is the effective length of the HNLF fiber given as $L_{eff} = \frac{1-\exp(-\alpha L_{HNLF})}{\alpha}$ [19]. Considering (10), it is clear that the operation range for measuring an optical pulse width can be extended by maximizing any or all of listed parameters. By using XPM simulations the dynamic range of the measurement system was estimated for practically achievable lower and upper limits for the following parameters. HNLF lengths were considered with the lower limit as L_{HNLF} = 20 m and L_{HNLF} = 1 km as the upper limit. We also considered a maximum available EDFA saturated output power ~40 dBm. The results of these simulations are summarized in Fig. 9.

From Fig. 9(a) we can see that the minimum pulse width that could be measured with the hardware is 250 fs and can be achieved using L_{HNLF} = 50 m and 15 dBm EDFA. As mentioned above, the resolution of this method is 0.25 ps, hence by using this hardware, the minimum possible pulse width can be measured as 250 fs. However, the device range can be extended to measure optical pulse widths well beyond 10 ps FWHM. If using L_{HNLF} = 20 m and 38 dBm EDFA or L_{HNLF} = 1 km and 21 dBm EDFA the device can be used to measure an optical pulse within the region of 10 – 40 ps as shown in Figs. 9(b) and 9(c), respectively. For pulses longer than 40 ps, the accumulated non-linear phase on the counter-propagating signal is significant, limiting the measureable effective non-linear phase shift of the system, highlighting the significant role of the repetition rate in this scheme. The device can be also easily reconfigured for pulse width measurements beyond a 40 ps range, by lowering the repetition rate, however for this regime, high speed electronics may be a more attractive option.

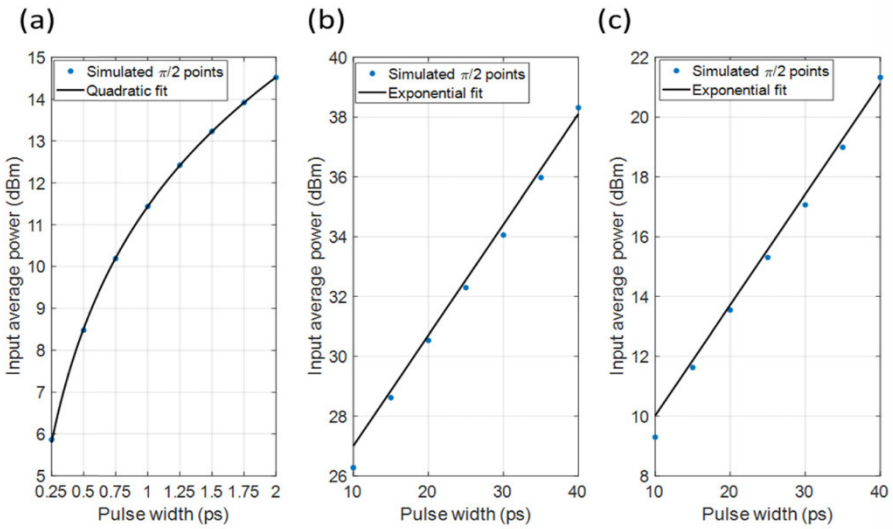

Fig. 9. Device parameters selection. (a) pulse width measurements below 2 ps: L_{HNLF} = 50m, EDFA saturated output 15 dBm; pulse width measurements below 100 ps: (b) L_{HNLF} = 20 m, EDFA saturated output 38 dBm or (c) L_{HNLF} = 1 km, EDFA saturated power 21 dBm.

6. Conclusion

We have presented an all-fiber non-linear interferometric method for determining optical pulse widths using measurements of average power using slow detectors. The approach is

Optics EXPRESS

applicable where Gaussian or $sech^2$ pulse envelopes can be assumed and the internal phase structure is slowly varying (for example in dispersive communications links). Pulses in the range of 2–10ps were successfully characterized experimentally. The dynamic range of the proposed method is limited by available hardware, with realistic limits of 250 fs to 40 ps. The method may find its use in distributed networks or as a bolt-on to optical systems using ultra-short pulse sources. This fiber device can be also implemented as an integrated non-linear Sagnac or Mach-Zehnder interferometer using integrated optical platforms, including silicon on insulator (SOI), where mode volumes can be small and non-linear coefficients can be very high, i.e. 307 $(Wm)^{-1}$, potentially leading to improvements in device miniaturization, stability and power [22].

Funding

Commonwealth Scholarship Commission United Kingdom (CSC – PKCA-2016-90); European Union Horizon 2020 research and innovation program under the Marie Skłodowska-Curie Grant (734331); Natural Sciences and Engineering Research Council of Canada.

References

1. G. Roelkens, U. Dave, A. Gassenq, N. Hattasan, Chen Hu, B. Kuyken, F. Leo, A. Malik, M. Muneeb, E. Ryckeboer, D. Sanchez, S. Uvin, R. Wang, Z. Hens, R. Baets, Y. Shimura, F. Gencarelli, B. Vincent, R. Loo, J. Van Campenhout, L. Cerutti, J.-B. Rodriguez, E. Tournie, Xia Chen, M. Nedeljkovic, G. Mashanovich, Li Shen, N. Healy, A. C. Peacock, Xiaoping Liu, R. Osgood, and W. M. J. Green, "Silicon-based photonic integration beyond the telecommunication wavelength range," IEEE J. Sel. Top. Quantum Electron. **20**(4), 394–404 (2014).
2. W. Zhong, M. Wu, C. W. Chang, K. A. Merrick, S. D. Merajver, and M. A. Mycek, "Picosecond-resolution fluorescence lifetime imaging microscopy: a useful tool for sensing molecular interactions in vivo via FRET," Opt. Express **15**(26), 18220–18235 (2007).
3. R. Trebino and D. J. Kane, "Using phase retrieval to measure the intensity and phase of ultrashort pulses: frequency-resolved optical gating," J. Opt. Soc. Am. A **10**(5), 1101–1111 (1993).
4. R. Trebino, "Frequency Resolved Optical Gating: The Measurement of Ultrashort Laser Pulses," Kluwer Academic (2002).
5. D. J. Kane, "Real-Time Measurement of Ultrashort Laser Pulses Using Principal Component Generalized Projections," IEEE J. Sel. Top. Quantum Electron. **4**(2), 278–284 (1998).
6. C. Iaconis and I. A. Walmsley, "Spectral phase interferometry for direct electric-field reconstruction of ultrashort optical pulses," Opt. Lett. **23**(10), 792–794 (1998).
7. S. P. Gorza, P. Wasylczyk, and I. A. Walmsley, "Spectral shearing interferometry with spatially chirped replicas for measuring ultrashort pulses," Opt. Express **15**(23), 15168–15174 (2007).
8. T. Hori, N. Nishizawa, T. Goto, and M. Yoshida, "Experimental and numerical analysis of widely broadened supercontinuum generation in highly nonlinear dispersion-shifted fiber with a femtosecond pulse," J. Opt. Soc. Am. B **21**(11), 1969–1978 (2004).
9. I. G. Cormack, W. Sibbett, and D. T. Reid, "Rapid measurement of ultrashort-pulse amplitude and phase from a two-photon absorption sonogram trace," J. Opt. Soc. Am. B **18**(9), 1377–1382 (2001).
10. M. D. Thomson, J. M. Dudley, L. P. Barry, and J. D. Harvey, "Complete pulse characterization at 15 μm by cross-phase modulation in optical fibers," Opt. Lett. **23**(20), 1582–1584 (1998).
11. P. A. Lacourt, M. Hanna, and J. M. Dudley, "Broad-Band and Ultrasensitive Pulse Characterization Using Frequency-Resolved Optical Gating via Four-Wave Mixing in a Semiconductor Optical Amplifier," IEEE Photonics Technol. Lett. **17**(1), 157–159 (2005).
12. L. Lepetit, G. Ch'eriaux, and M. Joffre, "Linear techniques of phase measurement by femtosecond spectral interferometry for applications in spectroscopy," J. Opt. Soc. Am. B **12**(12), 2467–2474 (1995).
13. C. Dorrer and I. Kang, "Linear self-referencing techniques for short-optical-pulse characterization," J. Opt. Soc. Am. B **25**(6), A1–A12 (2008).
14. F. Li, Y. Park, and J. Azana, "Linear characterization of optical pulses with durations ranging from the picosecond to the nanosecond regime using ultrafast photonic differentiation," IEEE/OSA. J. Lightwave Technol. **27**(21), 4623–4633 (2009).
15. A. Pasquazi, M. Peccianti, Y. Park, B. E. Little, S. T. Chu, R. Morandotti, J. Azaña, and D. J. Moss, "Sub-picosecond phase-sensitive optical pulse characterization on a chip," Nat. Photonics **5**(10), 618–623 (2011).
16. M. A. Foster, R. Salem, D. F. Geraghty, A. C. Turner-Foster, M. Lipson, and A. L. Gaeta, "Silicon-chip-based ultrafast optical oscilloscope," Nature **456**(7218), 81–84 (2008).
17. J. Y. Yang, L. Zhang, X. Wu, O. F. Yilmaz, B. Zhang, and A. E. Willner, "All-optical chromatic dispersion monitoring for phase-modulated signals utilizing cross-phase modulation in a highly nonlinear fiber," IEEE Photonics Technol. Lett. **20**(19), 1642–1644 (2008).
18. N. J. Doran and D. Wood, "Nonlinear-optical loop mirror," Opt. Lett. **13**(1), 56–58 (1988).

Optics EXPRESS

19. G. P. Agrawal, "Nonlinear Fiber Optics," 4th ed. Academic Press, Boston (2007).
20. Y. Miyoshi, S. Takagi, S. Namiki, and K. I. Kitayama, "Multiperiod PM-NOLM With Dynamic Counter-Propagating Effects Compensation for 5-Bit All-Optical Analog-to-Digital Conversion and Its Performance Evaluations," IEEE/OSA. J. Lightwave Technol. **28**(4), 415–422 (2010).
21. L. Poti, E. Lazzeri, G. Meloni, A. Bogoni, and G. Prati, "All-Optical Processing by Means of Cross-Phase-Modulation-Based PM-NOLM Interconnected Structures," IEEE J. Sel. Top. Quantum Electron. **14**(3), 580–586 (2008).
22. J. Leuthold, C. Koos, and W. Freude, "Nonlinear silicon photonics," Nat. Photonics **4**(8), 535–544 (2010).